Analysis of prompt fission neutrons in $^{235}U(n_{th},f)$ and fission fragment distributions for the thermal neutron induced fission of ^{234}U

A. Al-Adili[1,a], D. Tarrío[1], F.-J. Hambsch[2,b], A. Göök[2], K. Jansson[1], A. Solders[1], V. Rakopoulos[1], C. Gustafsson[1], M. Lantz[1], A. Mattera[1], S. Oberstedt[2], A. V. Prokofiev[1], M. Vidali[2], M. Österlund[1], and S. Pomp[1]

[1] *Department of Physics and Astronomy, Uppsala University, Sweden*
[2] *EC-JRC - Institute of Reference Materials and Measurements (IRMM), Geel, Belgium*

Abstract. This paper presents the ongoing analysis of two fission experiments. Both projects are part of the collaboration between the nuclear reactions group at Uppsala and the JRC-IRMM. The first experiment deals with the prompt fission neutron multiplicity in the thermal neutron induced fission of $^{235}U(n,f)$. The second, on the fission fragment properties in the thermal fission of $^{234}U(n,f)$.

The prompt fission neutron multiplicity has been measured at the JRC-IRMM using two liquid scintillators in coincidence with an ionization chamber. The first experimental campaign focused on $^{235}U(n_{th},f)$ whereas a second experimental campaign is foreseen later for the same reaction at 5.5 MeV. The goal is to investigate how the so-called saw-tooth shape changes as a function of fragment mass and excitation energy. Some harsh experimental conditions were experienced due to the large radiation background. The solution to this will be discussed along with preliminary results.

In addition, the analysis of thermal neutron induced fission of $^{234}U(n,f)$ will be discussed. Currently analysis of data is ongoing, originally taken at the ILL reactor. The experiment is of particular interest since no measurement exist of the mass and energy distributions for this system at thermal energies. One main problem encountered during analysis was the huge background of $^{235}U(n_{th},f)$. Despite the negligible isotopic traces in the sample, the cross section difference is enormous. Solution to this parasitic background will be highlighted.

1 Introduction

The Uppsala group has a few ongoing projects investigating nuclear fission, e.g. on independent fission yields, high precision cross sections and fission-fragment properties [1]. In recent years the group has also started new collaborations with colleagues from JRC-IRMM to measure prompt fission neutrons. This work discusses the analysis of two ongoing works on $^{235}U(n_{th},f)$ and $^{234}U(n_{th},f)$.

[a] e-mail: ali.al-adili@physics.uu.se
[b] e-mail: franz-Josef.HAMBSCH@ec.europa.eu

1.1 Prompt fission neutron multiplicity

The share of excitation energies between the fission fragments (FF) is of importance for understanding nuclear fission. In particular how the excitation energies (viz. neutron emission) varies as a function of incident neutron energy. The nuclear data community lacks conclusive data to address this issue, although some experimental data supports an increasing $\overline{\nu}(A)$ from the heavy fragments [2]. However, it seems also that theoreticians have agreed to disagree on the explanation of these observations. Certainly, more data are needed to understand the saw-tooth behavior at higher E_n. In addition, systematic studies on a few reactions and correlations between fragment+neutron characteristics could possibly contribute to a better modeling of the neutron emission. The current experimental activity on measuring $\overline{\nu}(A)$, is a feasibility test for a future larger systematic measurement campaign. A first step was to measure ^{235}U(n_{th},f) at the JRC-IRMM Van De Graff accelerator, and this will be compared to a future run at E_n = 5.5 MeV.

1.2 Thermal fission of a fertile system

The second part of the paper concerns data on ^{234}U(n_{th},f) originally measured at the reactor of the Institut Laue-Langevin (ILL) in Grenoble, France. The experiment was performed in 1999 using a conventional Twin Frisch-Grid Ionization Chamber (TFGIC) in conjunction with an analogue data acquisition system. The aim was to measure, for the first time, the fission mass yield, angular- and energy distributions of ^{234}U(n,f) at sub-thermal energy, much below the fission threshold. A cold neutron beam was used to induce fission in the main ^{234}U target and separately in a ^{235}U target for calibration purposes. Unfortunately some problems in the collected data jeopardized the extraction of useful results. Here, some 15 years later, new solutions are attempted to save what can be saved from the data. More details about those challenges will be discussed in sect. 3.

2 Project 1: $\overline{\nu}(A)$ for ^{235}U(n_{th},f)

As commonly known, measuring neutrons is not straightforward. In this work we are forced to detect them indirectly through their recoil to a proton. From the recoil energy the generated light output is extracted and compared to other signal shapes. The shape of the induced signal is related to the sort of particle giving rise to it. In such a way, one could separate gammas from neutrons for instance. The challenges do not stop here, because not all neutrons will have equal chances of getting detected. They even show a dependence on the incoming neutron energy. The internal detector efficiency has to be quantified e.g. by measuring a known standard spectrum which in this case comes from ^{252}Cf(sf). Once a neutron is identified (and successfully distinguished from scattered neutrons), we look for a coincidence with a fission fragment from the ionization chamber. If we found one, a game of kinematics starts to reconstruct the scene to reveal what angle and energy the neutron obtained when ejected. Once all observables are in place we ought to look for correlations that might lead to interesting insights.

2.1 Simulations of the background in the thermal measurement

Prior to the measurement, extensive simulations were performed with the FLUKA code [3] in order to ensure a minimum contribution from beam neutrons. Figure 1 shows the schematic experimental setup with the TFGIC and the neutron detectors (ND). The proton beam is impinging on a Li neutron-converter giving rise to 0.5 MeV neutrons. Paraffin was used to thermalize those neutrons before irradiating a 117 μg/cm^2 ^{235}U target placed in the centre of the chamber cathode. The chamber is

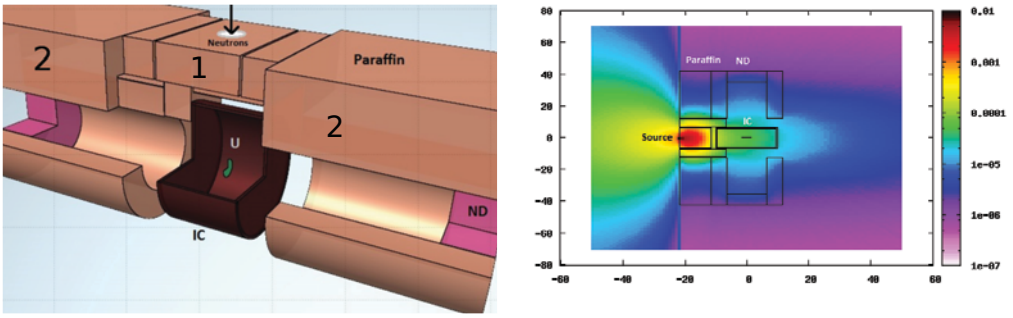

Figure 1. Left: The geometry simulated in FLUKA prior to the first experiment in 2014. Paraffin was used to thermalize the neutron beam. Right: The neutron flux density for the thermalized neutron beam.

tilted 90° to the neutron beam. The fission fragments are detected when they ionize the chamber gas (P-10 at 1.05 bar pressure) and the liberated electrons are collected on the anode plates. The neutrons are anisotropically emitted in the laboratory frame with preference towards the motion of the fully accelerated FF. The neutron detectors are placed on each side of the chamber in order to detect the FF with the highest mass-, energy and angular resolution (due to minimum energy losses in the target). Paraffin and Lead were planned to be used to protect the detectors from unwanted background from the neutron field. The neutron fluxes in the target and neutron detectors were estimated (See Fig. 1). A balance had to be achieved between the n-FF coincidence rate and the acceptable level of neutron background in the detectors. The best combination found was to use a low energetic neutron beam of 0.5 MeV together with large amounts of paraffin, because the NE213-based scintillator is practically transparent to thermal neutrons. The neutron flux at the U target was estimated to be roughly 10^4 n/cm^2 s, of which 93% are below 100 keV. In total this corresponds to about $\approx$ 50 ff/s. The solid angle of the neutron detectors, at 35 cm distance, is roughly 1% which gives a coincidence rate of about 0.5 coincidences/s. About 2.4 neutrons are emitted on average per fission event, but this is compensated by the neutron detector intrinsic efficiency which is about 30% on average. Thus, about half a million neutron-FF coincidences were to be expected in 15 days of stable beam-time at 5 μA. The background level in the neutron detectors are in the order of a million n/s. However, only a small fraction are above the detection threshold of the liquid scintillator. Because the chamber provided the fission trigger and considering the time of flight of the fission neutrons, the background level in the detectors was regarded to be of no concern for the thermal measurement.

2.2 Experiments and analysis

The experimental data was collected using a digital data acquisition system. The fission fragment energies and angles were obtained from the chamber signals. The neutron energy is derived from the time-of-flight (ToF) calculated as the time difference between the cathode signal and the neutron detector pick-off signal. Hence, the signal from both chamber and neutron detectors were digitized and stored for off-line analysis. The neutron multiplicity is estimated by counting the number of times a coincidence was registered between the FF and the neutron detector. The experimental and analysis procedure is very much similar to the work of Ref. [4]. First, ^{252}Cf(sf) was measured using the identical experimental setup. By utilizing the Mannhart evaluation for the neutron spectrum, one can determine the detector efficiency function. In order to estimate the level of neutron scattering, the

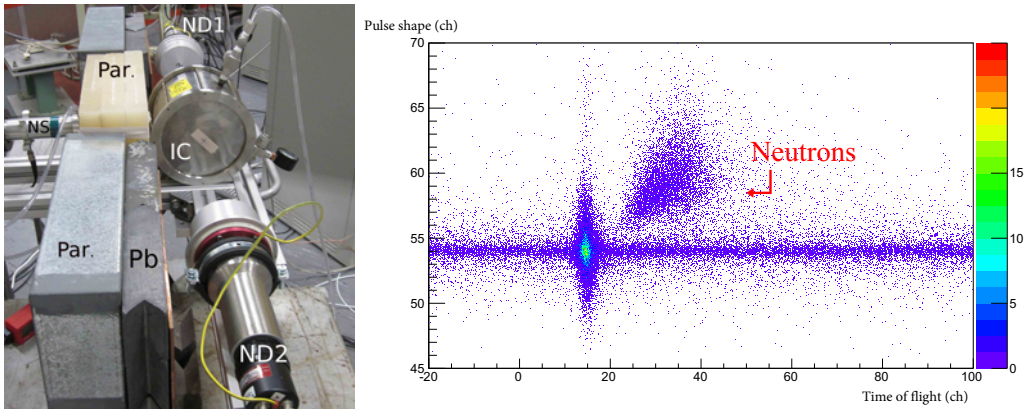

Figure 2. Left: The experimental setup. The neutron source (NS) can be seen along with the shielding material (Pb), moderator (Paraffin), the IC and the two ND. Right: The raw data from the ^{235}U run neutron detector showing gammas and neutrons.

surrounding material was removed in one run and ^{252}Cf was remeasured. In this way one can later study the impact of the shielding material on the neutron spectrum and to understand the scattering component from the Prompt Fission Neutron Spectrum (PFNS). An additional reduction to the effect of scattered neutrons, is done by analyzing the neutron detector pulse height versus ToF and looking for the maximum transfer of energy to the recoil protons in the scintillator.

During the measurement, up to 10^5 γ/s were registered in the ND. Most of which came from the beam or from neutron capture in hydrogen. Luckily, due to the possibility of neutron gamma separation based on pulse shape (PS), one may get rid of the gamma component. Some raw data are shown in Fig. 2 and the gammas are appearing uncorrelated with time and have a particular signal fall-time (zero-crossing method). However neutrons are correlated with time since they are in coincidence with the trigger from the fission chamber. Note also the prompt fission gammas are also in coincidence with the fission fragments in the chamber. By means of Gaussian fitting as a function of signal height, one may retrieve the border line between gammas and neutrons as seen in Fig. 3. The timing resolution can be looked for in the prompt fission gamma peak and is slightly above 1 ns. Despite the resolution limit from the sampling rate (2.5 ns/sample) digital interpolations allow for obtaining a better timing resolution. The lower plots of Fig. 3 show the ToF spectra before and after PS discrimination. The green line shows the neutron energy after discrimination against gammas and a ToF cut. From the tof spectrum, the neutron energy is calculated following non-relativistic kinematics. The resulting neutron spectra for the two detectors are shown in the left plot of Fig. 4 together with the Mannhart evaluation. The agreement between the two detectors is very good. However the energy calibration is still under investigation so the two detectors might not have the same threshold. The neutron detector efficiency (shown as an example in the right plot of Fig. 4) is determined from the Cf measurement by dividing the calculated neutron energy spectrum with the Mannhart evaluation. The solid angle has to be accounted to estimate the detection efficiency. The detector efficiency is dependent on the threshold in the detector as shown in a simulation in the figure for different pulse height [5]. Ongoing work is now focused on the energy calibration to ensure the same threshold in both detectors.

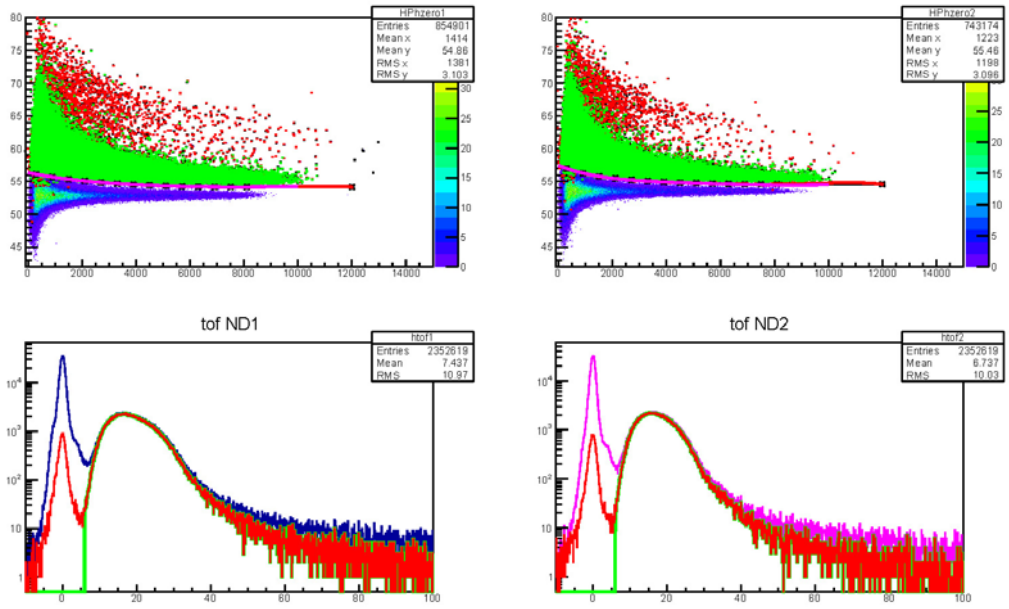

Figure 3. Upper :The neutron gamma separation by use of the pulse shape discrimination technique. Gaussian fits as a function of pulse height in the ND give the separation line between prompt gamma and prompt neutrons. Lower: The ToF spectra before and after pulse shape (PS) discrimination. The green lines show the neutron energy after discrimination against gammas and a ToF cut.

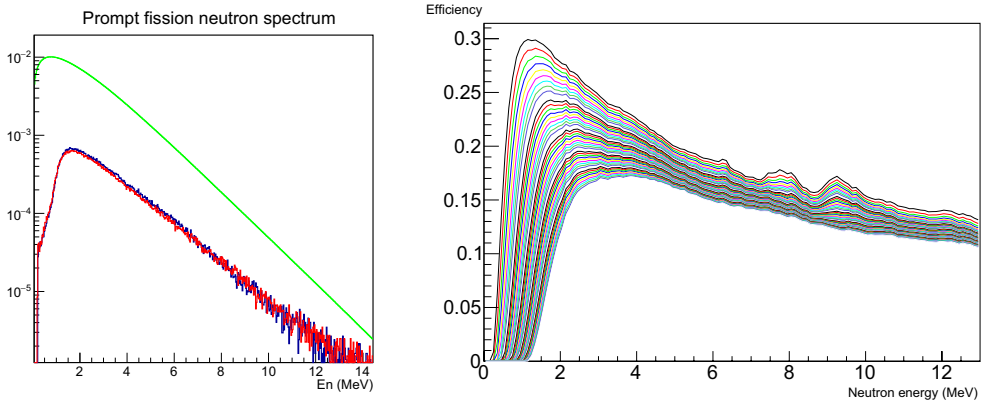

Figure 4. Left: The ^{252}Cf neutron spectra from the two detectors together with the Mannhart evaluation. Right: The detector efficiency as a function of detector threshold (GEANT simulation from Ref. [5]).

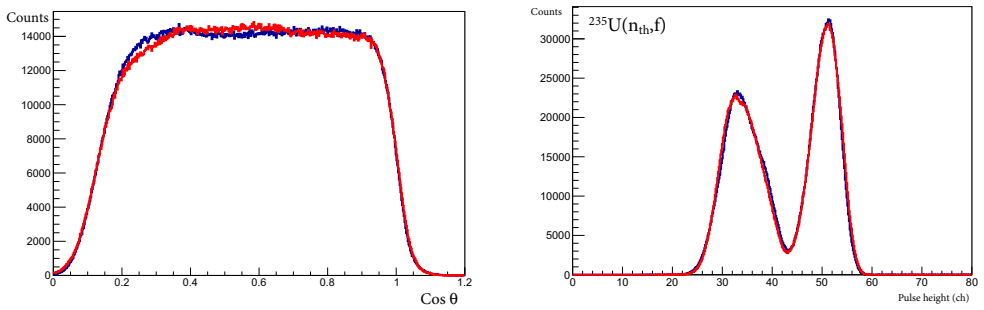

Figure 5. Left: The cosine distribution of the fission fragments from both sample and backing sides. Right: The pulse-height (energy) distributions from sample and backing sides.

2.3 Preliminary results

We are still in the process of ensuring the quality of the neutron data. Once the data are in optimum shape the fission fragment correlation study can be finalized. However preliminary, the provisional distributions have been studied to obtain an overall check. Some rough analysis on the ^{235}U fragment data was done and the distributions show a decent behavior. The cosine distribution is plotted for the two chamber sides in Fig. 5 together with the pulse height distributions (proportional to the fragment energy). A decent matching is seen, despite improvements will enhance the agreement between the two sides. Figure 6 shows a preliminary plot on the coincidence condition between the two detectors and the chamber. To the left and in the middle, are the two provisional mass distributions for ^{235}U(n$_{th}$,f) with (green, pink) and without (blue, red) coincidence condition. The asymmetric distributions are from the coincidence condition where the light fragments seem to emit more neutrons. The ratio between those two distributions give a rough idea on the saw-tooth trend (see right plot of Fig. 6). Albeit the roughness of the provisional plots and the discrepancy between the two detectors we are optimistic that the data look reasonable. Final data analysis is ongoing and preparations for the next campaign is also under exploration.

2.4 Testing and preparations for measuring at E_n = 5.5 MeV

A test run was performed later in 2015 on the 5.5 MeV case, also with two liquid scintillators and a Frisch-Grid ionization chamber. The aim was to investigate the background conditions and to compare roughly with the thermal measurement. MCNP and FLUKA simulations were performed before the experiment to estimate the neutron fields and to optimize the experimental setup. Due to problems with the beam, statistics became an issue for the 5.5 MeV test run and focus was instead put on benchmarking the simulations with different shielding conditions/materials. Shielding materials such as Pb, Cu and Paraffin were all used in different configurations and thicknesses. A throughout benchmarking is ongoing between the different simulation codes and the experimental data.

3 Project 2: Fission properties of ^{234}U(n$_{th}$,f)

3.1 Experiments

In 1999, neutrons from the ILL reactor were irradiating the Uranium sample inside a Frisch-grid ionization chamber. Two different targets were used separately during the experimental campaign; one

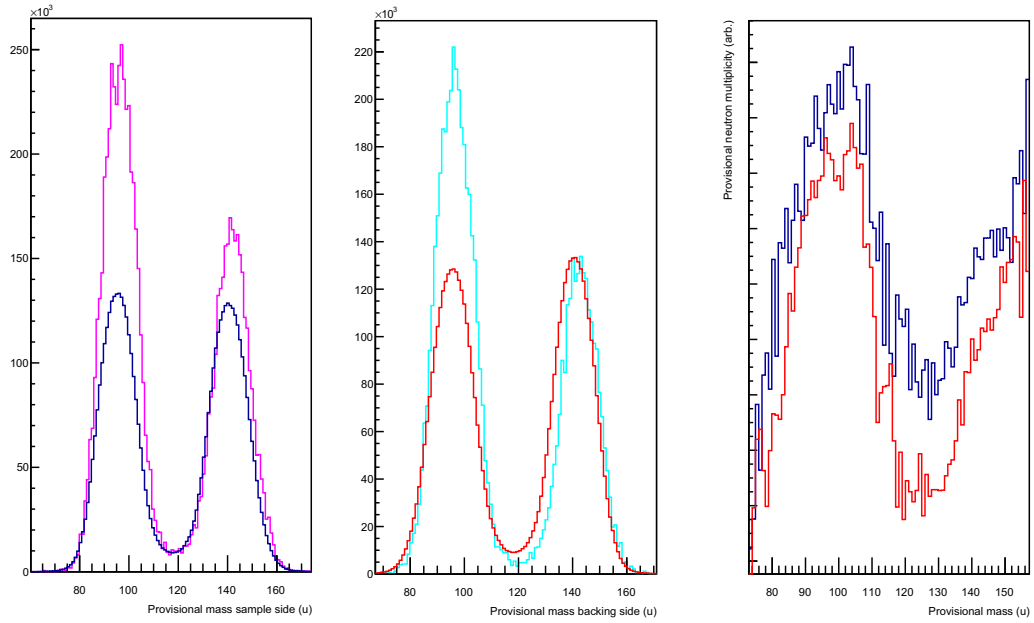

Figure 6. Left and middle: The provisional mass distributions from the two chamber sides. The more symmetric distributions show the non-coincidence mode whereas the asymmetric show the coincident events between neutrons and fission fragments. The ratio between the distributions is seen in the right plot and comprised a preliminary saw-tooth trend.

^{234}U sample for the main measurement and another natural uranium target for the reference measurement with ^{235}U. Unfortunately, two problems affected the data and have implied a rather cumbersome analysis of these data:

1. **Fission events from the reaction ^{235}U(n_{th},f).** The ^{234}U sample used for irradiation has a contamination of 0.07% of ^{235}U residues. Despite the negligible trace, the thermal fission cross section is much larger (584 barn instead of 0.067 barn). Due to this difference in fission cross section a larger ^{235}U(n_{th},f) background was contaminating the desired ^{234}U data (roughly 87%). The problem arises in the kinematics calculations since the mass of the fissioning compound nucleus (m_{cn}) is unknown yet an important parameter. With a large background of ^{235}U(n,f), m_{cn} is in fact to a large extent 236 u rather than 235 u. Proper treatment of this background was necessary. One possible solution is to randomize m_{cn}, event-by-event wise, between the two values (based on the ratio of cross sections) and analyze the data in a Monte Carlo manner. Another solution is to utilize the reference measurement to subtract for the unwanted background. The latter approach was found better suited for this application. The ^{235}U data was treated in the same way as the background data in the ^{234}U data set, namely by using m_{cn}=235 and the neutron multiplicity of $\bar{\nu}_{234}$(A).

2. **Fission product range in the gas.** Due to some restricting conditions, a CF_4 counting gas was used at a reduced gas pressure. Unfortunately, the high energetic ions were not fully stopped (light fission products). As a result, a clear artefact can be seen in the plots of energy versus emission angle. This problem implied that the angle determination of the light ions could not be extracted with confidence and had to be determined otherwise. The solution was to use only the emission angle from the complementary heavy fragment in each fission event, since these have lower kinetic energy and have obtained full stopping range in the gas. In addition, the data with smaller emission angles, corresponding to non-fully measured pulse height had to be excluded from the full analysis.

In the following section, the ongoing search for solutions to these problems is explained.

3.2 Analysis

The analysis of the fission fragment data followed the procedure described in Ref. [6]. The conservation of mass and momentum provides the means of calculating the pre-fission neutron emission distributions. In order to address the first issue of sect. 3.1, the analysis procedure was as follows:

1. The absolute energy calibration was performed by analyzing the ^{235}U(n_{th},f) data. The experimental parameters were fine-tuned to reach the literature values on the average total kinetic energy (TKE = 170.5 MeV) and average heavy mass of 139.6 u. m_{cn} = 236 is used along with $\overline{\nu}_{235}$(A) [7].

2. The ^{234}U(n_{th},f) data was analyzed with m_{cn} = 235 and $\overline{\nu}_{234}$(A) [8].

3. The ^{235}U(n_{th},f) data was now re-analyzed assuming it is ^{234}U(n_{th},f), i.e. with m_{cn} = 235 and $\overline{\nu}_{234}$(A).

4. The background subtraction is performed on item (2), by subtracting item (3) from it after scaling with the fission cross section and mass. The fission rate is given by the sum of all fissioning isotopes:

$$FR = (\sigma_{234} \times N_{234} + \sigma_{235} \times N_{235} + \sigma_{other} \times N_{other})\,\Phi \quad , \tag{1}$$

where N denotes the number of atoms, σ is the fission cross section and Φ is the neutron flux. The main contributions come from the two first isotopes, whereas the other are negligible. Therefore, the fraction of fissions coming from ^{235}U(n,f) is:

$$FR_{235} = \frac{\sigma_{235} \times N_{235}}{\Sigma\{\sigma \times N\}} \approx \frac{584b \times 0.077\%}{0.067b \times 99.923\% + 584b \times 0.077\%} \quad \approx 87\% \tag{2}$$

Although, the 99.923 % includes all other isotopes but ^{235}U, using σ_{234} is a fairly good approximation.

3.2.1 α Pile-up

The ^{234}U sample had a pile-up rate of about 10^5 α/s. These alpha particles affect also the background data (i.e both ^{234,235}U(n_{th},f)). Therefore, in view of the needed background subtraction stressed in point 1, sect. 3.1 the background has to be affected by the same pile-up signals. The response of the

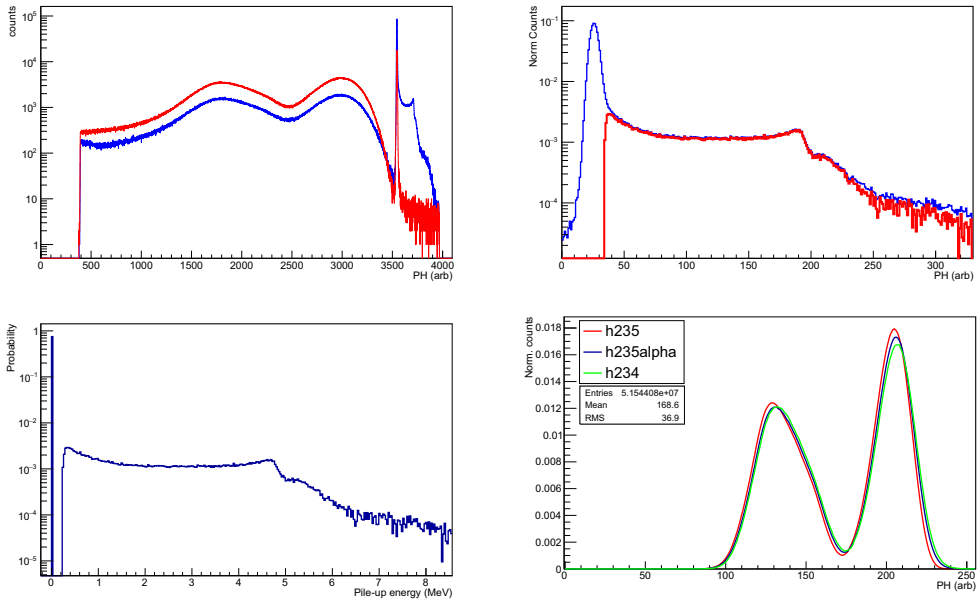

Figure 7. a) The α pile up in ^{234}U (blue) in contrast to the pulse height from ^{235}U (red), together with the signal from the precision pulse generator (at ch 3500). b) The α pile up contribution (red) deduced from the affected pulser signal. c) The probability density function (PDF) of α pile up signals, generated from the pulser response function. 30% is the estimated α pile up rate. d) The pulse height distributions for ^{234}U (green), the background run ^{235}U (red) and the simulated α pile up affected ^{235}U background (blue).

detector to the pile-up can be studied on the precision pulse-generator, originally used for electronic-drift monitoring. Since the pulser gives a well-defined signal, the impact of the alpha pile-up is nicely visible. Figure 7a shows the pulse-height distributions of ^{234,235}U(n_{th},f) and the pulser at channel 3500 (note the pile up on the pulser in the case of ^{234}U (blue line)). The pulser signal was used as a probability density function (PDF) to simulate the α pile up in the background data. The α pile up contribution is seen in Fig. 7b. About 70 % of the events are free from pile-up. The PDF was created by converting the α contribution to energy (see Fig. 7c) and adding a zero channel with the amplitude 1-Integral(α contribution). In the last step, a random generator was used to sample from the generated PDF and thus emulate the pile-up process by adding the signal to the anode signals stochastically event-by-event. The result is shown in Fig. 7d where the pulse height distribution is shown for ^{234}U (green line) and ^{235}U (red line). By adding the simulated α pile up, the ^{235}U distribution (blue line) is closer to the naturally affected ^{234}U data (which in turn is dominated by the background of ^{235}U).

3.2.2 Emission angle and energy losses

The two signals used from the ionization chamber are the anode and sum (anode+grid) signals. After the grid inefficiency correction [9, 10] the angular distributions were determined via the summing method [11].

A zoomed plot is shown on the light fragments in Fig. 8 where the effect of the second issue of sect. 3.1 is clearly visible. The fragments do not acquire their full stopping range and thus accumulate

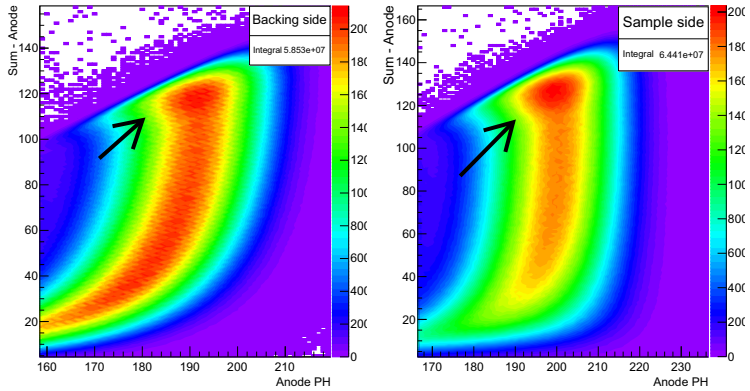

Figure 8. a) $PH_\Sigma - PH_A$ versus PH_A, used to extract the emission angle (See text for details). Note the range issue at larger PH_Σ values (sect. 3.1).

for smaller emission angles and high energies. The $\overline{X}/D$ distribution for all light fragments will be affected by a too small range. The resulting $\cos(\theta)$ distributions from the two chamber exhibits an overshoot at angles close to $\cos(\theta)$=1 especially for the sample side. In addition the slope of the backing side seems to be too steep. The angular resolution in terms of Full Width at Half Maximum (FWHM) is 0.084. Because of the second issue of sect. 3.1, the angular resolution is determined only for $0.5 \leq \cos(\theta) \leq 0.85$. The best solution found to the range problem was to use the emission angle from the heavy fragment solely. Since the angular resolution seems to be fairly good, the uncertainty from doing so is relatively small.

The energy-loss correction is done on the mean anode pulse heights from both chamber sides as a function of $1/\cos(\theta)$. A linear fit is extrapolated to the intersection at the y-axis corresponding to an assumed ideal energy-loss free channel to which the pulse heights are then corrected to, depending on the emission angle. Due to the degraded angular resolution at higher angles, the final fragment mass calculation includes only events with $\cos(\theta) \geq 0.5$. In addition, due to the issue 2 of sect. 3.1, the angle is further restricted to $0.5 \leq \cos(\theta) \leq 0.85$.

3.2.3 Fragment-mass determination

The "pulse-height defect" (PHD) accounts normally for about 4 MeV reduction in the detected FF energy. It depends mainly on the fragment mass and energy, and can be corrected for by the parametrization from Ref. [12]. In this work, the PHD had to be larger (about 6-7 MeV) in order to obtain proper reference distributions. Probably this is due to the different conditions of this experiment compared to standard measurements performed at the JRC-IRMM (i.e. properties of the counting gas CF_4 compared to P-10 gas).

One critical step in the analysis is to estimate the neutron emission on an event-by-event basis. The neutron multiplicity of ^{235}U(n_{th},f) was obtained from Ref. [7]. The neutron multiplicity of ^{234}U was obtained as the average of ^{233}U and ^{235}U [13]. In addition to the mass dependence, the neutron multiplicity is dependent on the TKE. Both sawtooth shapes used in this work are shown in Fig. 9a.

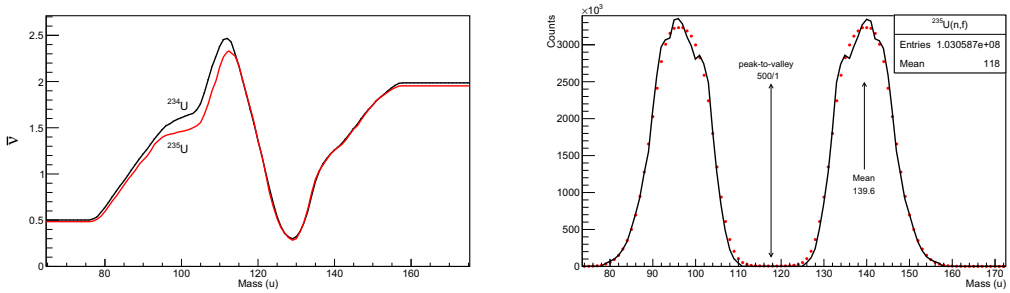

Figure 9. a) The neutron multiplicity for both systems. ^{235}U was obtained from Ref. [7]. ^{234}U was obtained from an average of ^{233}U and ^{235}U. b) the experimental mass distribution of ^{235}U(n,f) (red dots) compared to literature data from Ref. [14] (solid line).

The full kinematics necessary to determine the fragment masses are described in Ref. [8]. In this work, the equations are simplified since the neutron energy is about 0 MeV. The pre-neutron emission energy in the CM system can be calculated by:

$$E_{\mathrm{pre}}^{\mathrm{CM}} = \frac{A_{\mathrm{pre}}}{A_{\mathrm{pre}} - \nu\,(A, \mathrm{TKE})} E_{\mathrm{post}}^{\mathrm{LAB}} \tag{3}$$

The final pre-neutron emission fragment masses are calculated as:

$$A_{1,\mathrm{pre}} = A_{\mathrm{CN}} \cdot \frac{E_{2,\mathrm{pre}}^{\mathrm{CM}}}{E_{1,\mathrm{pre}}^{\mathrm{CM}} + E_{2,\mathrm{pre}}^{\mathrm{CM}}} \qquad \text{and} \qquad A_{2,\mathrm{pre}} = A_{\mathrm{CN}} \cdot \frac{E_{1,\mathrm{pre}}^{\mathrm{CM}}}{E_{1,\mathrm{pre}}^{\mathrm{CM}} + E_{2,\mathrm{pre}}^{\mathrm{CM}}} \tag{4}$$

The calculations above are repeated in an iterative loop where the newly calculated masses are always compared with the earlier determined. When the mass difference, $A_{\mathrm{new}} - A_{\mathrm{old}}$, in two sequential iterations is less than 1/16 amu the calculation is finished.

3.3 Preliminary results

In sect. 3.2 the analysis scheme was presented. In the first step, the calibration is done using ^{235}U(n_{th},f). The resulting mass distribution of the reference run is shown in Fig. 9b (full line), in comparison to the one of Ref. [14] (red dots). The peak-to-valley ratio between the peaks and the symmetric yield region is around 500 and the mass distributions are in relatively good agreement. Due to the limited mass resolution in the present experiment the finer structure is not reproduced.

In the second step,^{234}U(n,f) was analyzed and the resulting mass vs TKE is shown in Fig. 10a. In the third step and in order to subtract the background, the reference ^{235}U was re-analyzed with m_{cn} = 235 and $\bar{\nu}_{234}$. Fig. 10b shows the mass vs TKE. Note also that to the reference also a simulated α pile up (see sect. 3.2.1 for details) was added. Finally the background was subtracted from the 2-dimensional mass and TKE plot after scaling the background to the calculated fission rate (Fig. 10c).

Figure 11a shows the fission yields for ^{234}U(n,f) plus the background, the background normalized to the fission cross section, ^{235}U, and the background-subtracted ^{234}U(n,f). The difference between the two distributions is the assumed clean ^{234}U(n,f) mass yield. Figure 11b shows all cases compared to

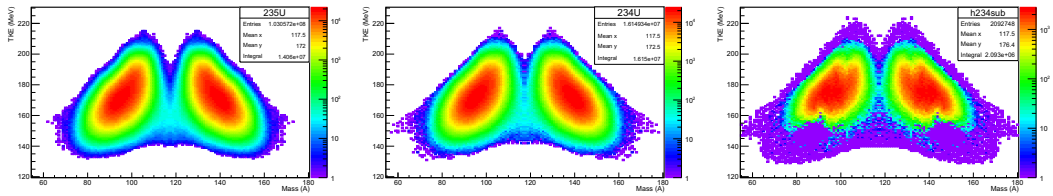

Figure 10. a) ^{234}U(n,f) including the 85% background of ^{235}U(n,f). b) ^{235}U, analyzed as ^{234}U(n,f) and normalized to the cross section. Note the number of entries which is the actual statistics and the integral which is the normalized number of events. c) The difference between the two distributions is the assumed clean ^{234}U(n,f) yield.

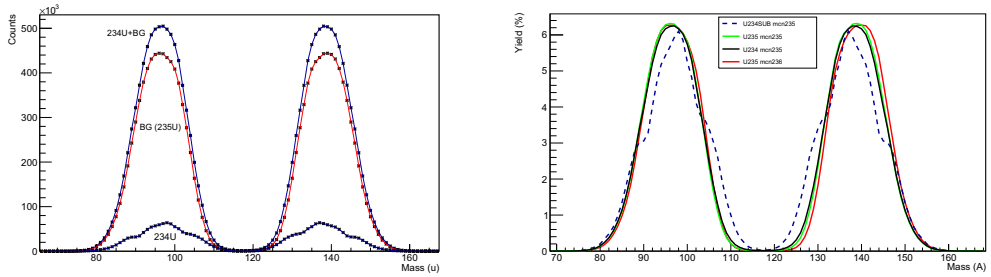

Figure 11. a) ^{234}U+background (BG) shown together with ^{235}U (Bg), analysed as ^{234}U(n,f) and normalized to the cross section. The difference between the two distributions is the assumed clean ^{234}U(n,f) mass yield. b) The mass distribution for ^{235}U analysed as ^{235}U(n,f) (red) and ^{234}U(n,f) (green). In addition ^{234}U(n,f) with (dashed) and without background subtraction (black).

each other, namely: The mass distribution for ^{235}U analyzed as m_{cn}=236 (red), ^{235}U(n,f) as m_{cn}=235 (green), ^{234}U(n,f) with (dashed) and without background subtraction (black). As seen already in Fig. 11c, unfortunately the final mass distribution of ^{234}U(n,f) has some problems and the solution to this is still under investigation.

Acknowledgements

The authors would like to thank CHANDA and EUFRAT for their financial support to perform these scientific works. The Van De Graff staff of the JRC-IRMM are acknowledged for their technical support and for providing the beam.

References

[1] Al-Adili, et al. Phys. Proc. **64**, 145 (2015).
[2] A. A. Naqvi, et al. Phys. Rev. **C34**, 218 (1986).
[3] T.T. Böhlen, et al., Nucl. Data Sheets **120**, 211 (2014).
[4] A. Göök, et al. Phys. Rev. **C90**, 064611 (2014).

[5] A. Göök, Private communication.
[6] C. Budtz-Jørgensen, et al. Nucl. Meth. Instr. **A258**, 209 (1987).
[7] A.C. Wahl, At. Data and Nucl. Data Tables **39**, 1 (1988).
[8] A. Al-Adili, et al. Phys. Rev. **C86**, 054601 (2012).
[9] A. Göök, et al. Nucl. Meth. Instr. **A664** 289 (2012).
[10] A. Al-Adili, et al. Nucl. Meth. Instr. **A673**, 116 (2012).
[11] A. Al-Adili, et al. Nucl. Meth. Instr. **A671**, 103 (2012).
[12] F.-J Hambsch, et al. Nucl. Meth. Instr. **A361**, 257 (1995).
[13] A. Al-Adili, et al. Phys. Proc. **47**, 131 (2013).
[14] G. Simon, et al. Nucl. Meth. Instr. **A286**, 220 (1990).